Electronic Supplementary Information (ESI)

A Self-Limiting Material Growth Triggered and Tunable by Force Through Piezocharge-induced Mineralization

Grant Kitchen[1,4], Bohan Sun[2,4], Mostafa Omar[2,4], Adebayo Eisape[3,4], Sung Hoon Kang[2,4,5]*

1. Department of Materials Science and Engineering, Johns Hopkins University, Baltimore, 21218, USA
2. Department of Mechanical Engineering, Johns Hopkins University, Baltimore, 21218, USA
3. Department of Electrical and Computer Engineering, Johns Hopkins University, Baltimore, 21218, USA
4. Hopkins Extreme Materials Institute, Johns Hopkins University, Baltimore, 21218, USA
5. Department of Materials Science and Engineering, Korea Advanced Institute of Science and Technology, Daejeon, 34141, Republic of Korea

Email: Sung Hoon Jang: shkang@jhu.edu

Table of Contents:

I. Supplementary Note 1: Analytical Model

Derivation of relationships between charge, thickness, and time

To derive analytical expressions for the evolution of the effective charge and mineral thickness, we started with following assumptions for the material system.

The driving force for the mineral ion attraction, adsorption, and mineral formation is the attraction between piezoelectric charges and mineral ions. While the magnitude of the generated charge is constant under cyclic loading with a constant amplitude, if the mineral layer is an electrical insulator then the effective charge that reaches through the mineral layer to surrounding mineral ions will decrease. As the minerals form, the effective charges are progressively shielded, decreasing the driving force for mineral ion attraction, adsorption, and mineral formation. Ultimately, the minerals will reach a saturation thickness as the driving force for further growth converges to zero. The initial condition at time zero will also be that the measured effective charge is at a maximum and the mineral thickness is zero. At infinite time, the steady-state mineral thickness will be at a maximum, and the effective charge will be zero. With these assumptions, we can write two differential equations for the effective charge and the mineral thickness with respect to time as below.

Change in effective charge over time:

$$\frac{dQ_{eff}}{dt} = -\alpha Q_{eff} \qquad \text{(Eq. S1)}$$

, where t is time, α is the proportionality constant, and Q_{eff} is the effective charge.

Change in mineral thickness over time:

$$\frac{dH}{dt} = -\beta H \qquad \text{(Eq. S2)}$$

, where t is time, β is the proportionality constant, and H is the mineral thickness.

Initial condition (time = 0):

$Q_{eff} = Q_0$ and $H = 0$

, where Q_{eff} is the effective charge, Q_0 is the initial charge, and H is the mineral thickness.

Steady-state condition (time = ∞):

$Q_{eff} = 0$
$H = H_f$

, where T_f is the saturation thickness.

From Eqs. (S1) and (S2) and these boundary conditions, the solutions for these differential equations becomes

$$Q_{eff}(t) = Q_0 \exp(-\alpha t) \quad \text{(Eq. S3)}$$

, where Q_{eff} is the effective charge, Q_0 is the initial charge, A is the proportionality constant, and t is time.

$$H(t) = H_f[1 - \exp(-\beta t)] \quad \text{(Eq. S4)}$$

, where H is the mineral thickness, H_f is the saturation thickness, β is the proportionality constant, and t is time.

The analytical model indicates that the decrease in effective charge follows an exponential relationship with material growth, and the maximum thickness is determined by the initial charge magnitude. As the initial charge is a function of the loading force and the piezoelectric coefficient, the analytical model indicates that force can be used to control the self-limiting growth thickness without changing the growth environment such as temperature, concentrations, or geometry.

II. Supplementary Note 2: Mineralization Procedure

SBF Preparation

To accelerate the mineralization process, two formulations of simulated body fluid (SBF) were prepared, 10× SBF-A and 10× SBF-B. The solutions were prepared using reagent-grade materials of NaCl, $CaCl_2$, $MgCl_2 \cdot 6H_2O$, $CaCl_2$, $NaHPO_4 \cdot 3H_2O$, and $NaHCO_3$ dissolved into deionized (DI) water as listed in (Table S1)[1–3]. All reagent materials were purchased from Sigma-Aldrich. 10× SBF-A was formulated to promote calcium-phosphate nucleation and 10× SBF-B was formulated to promote calcium-phosphate growth. The ionic concentrations were modified from SBF-A and SBF-B formulations by Habibovic *et al.*[1] by increasing the concentrations of each ionic species to increase the nucleation and mineralization rates[4].

Table S1 Ion concentrations of human blood plasma and simulated body fluids[1,2,3].

	Ion concentration (mM)							
	Na^+	K^+	Ca^{2+}	Mg^{2+}	Cl^-	HCO_3^-	HPO_4^2	SO_4^{2-}
Blood plasma	142	5.0	2.5	1.5	103	27.0	1.0	0.50
SBF	142	5.0	2.5	1.5	148	1.0	1.0	0.5
10× SBF	1030	5.0	25	5.0	1065	10	10	-
10× SBF-A	1430	-	25	15.0	1470	42	10	-
10× SBF-B	1408	-	25	3.0	1436	21	10	-

Each ionic species was added sequentially to DI water from left to right in (Table S1), allowing for each electrolyte to fully dissolve before adding the subsequent species. Solutions were prepared immediately before use to minimize the variance of the pH and solution stability between samples and refreshing cycles.

PVDF Sample Preparation

The piezoelectric polymer polyvinylidene fluoride (PVDF) was used as a substrate for the minerals (Manufacturer: Kureha). Sections of the PVDF were sealed with polyether ether ketone (PEEK) tape (McMaster-Carr 7263A81) to avoid leaving adhesive residue on the PVDF surface to create reference unmineralized areas of the PVDF substrate to accurately measure the thickness of the formed minerals. The PEEK tape regions were spaced 1 cm apart. A schematic and a taped sample are shown in (Fig. S1).

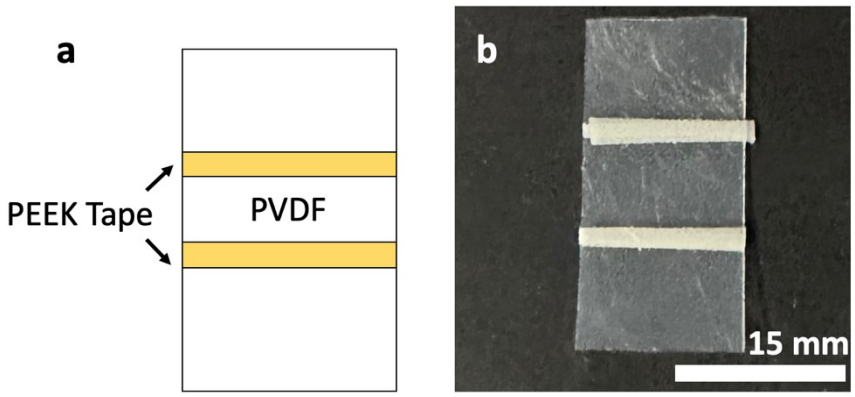

Fig. S1 Preparation of piezoelectric substrates. (a) Schematic of PVDF sample with PEEK tape sealed sections. (b) Picture of a PVDF sample with PEEK tape sealed sections.

The placement of the PEEK tape was selected to minimize the variance in mineral thickness and charge magnitude from boundary effects to improve the consistency and accuracy of the thickness and charge measurements.

Sample Loading

The taped PVDF sample was attached to an electrodynamic shaker (APS 2025E) and a load cell (McMaster-Carr 3487N29) to apply cyclic loading to the PVDF sample with controlled loading force and frequency. To control the SBF temperature, the PVDF sample and SBF chamber were placed within a surrounding water bath heated with immersion heaters (McMaster-Carr 4668T51) connected to a temperature controller and thermocouple system (Inkbird ITC-308S) to maintain a consistent target temperature. A schematic of this setup is shown in (Fig. S2).

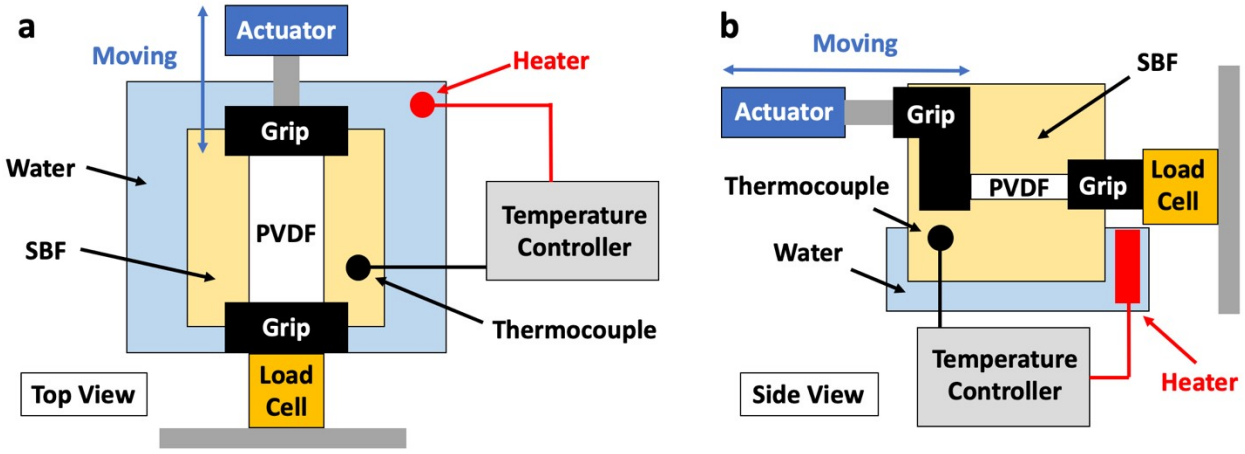

Fig. S2 Cyclic loading testing setup. (a) Schematic of the top view of the cyclic testing setup, with the piezoelectric PVDF sample connected to a load cell and an electrodynamic shaker and submerged in temperature controlled SBF. (b) Schematic of the side view of the cyclic testing setup.

The sample was mounted to the load cell and electrodynamic shaker during nucleation, mineral growth, and charge measurement tests. In addition, the load cell and electrodynamic shaker were connected to a computer and controlled with LabVIEW.

Mineral Nucleation

To nucleate the PVDF sample with calcium-phosphate, the PVDF sample was taped as in (Fig. S1) and mounted to the load cell and electrodynamic shaker as in (Fig. S2). After collecting the initial charge measurements by cyclically loading the sample in air, the sample was submerged in 10× SBF-A maintained at 25 °C for 24 hours. A schematic of this process is shown in (Fig. S3).

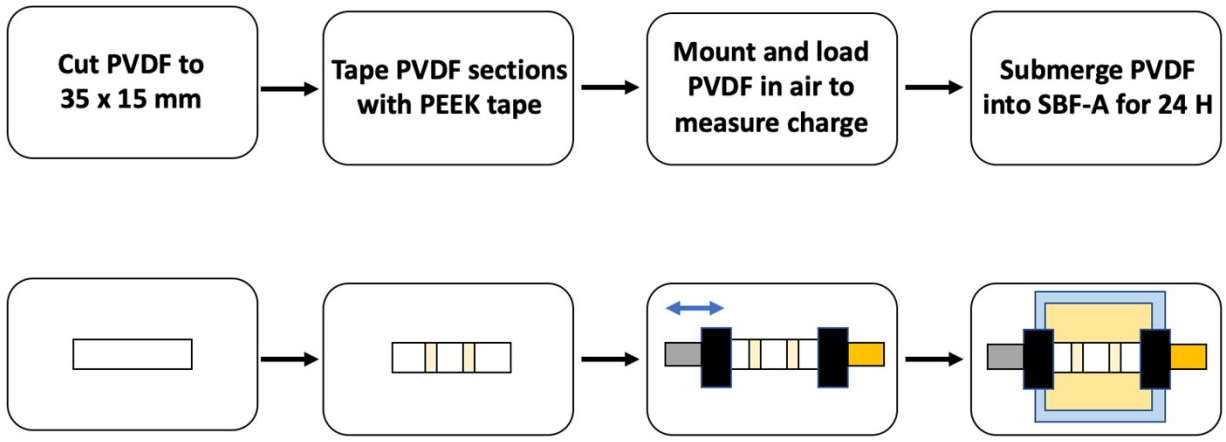

Fig. S3 Sample preparation, initial measurement, and nucleation procedure. The PVDF sample is taped, mounted, and tested before being submerged into SBF-A to seed the PVDF sample with calcium-phosphate nuclei. The top row shows the description of the procedure and the bottom one shows the schematic of the procedure.

Following the 24 hour unloaded nucleation period, the PVDF sample remains mounted and the SBF-A is replaced with a fresh solution SBF-B for mineral growth.

Mineral Growth

To grow the calcium-phosphate minerals on the seeded PVDF, the sample was mounted to the load cell and electrodynamic shaker. Then, the PVDF was submerged in 10× SBF-B maintained at 25 °C and cyclically loaded for 24 hours at a fixed frequency as the generated charges attract mineral ions to adsorb and form calcium-phosphate minerals. Following the 24-hour growth period, the SBF-B was removed and the PVDF was cyclically loaded in air to measure the effective charge through the mineral layers. The PVDF is then dismounted from the load cell and electrodynamic shaker and the PEEK tape is removed. The mineral thickness is then measured using a laser profiler (Keyence VK-X100). Following the charge and thickness measurements, the growth process and measurements were repeated multiple times until the steady-state maximum mineral thickness was achieved.

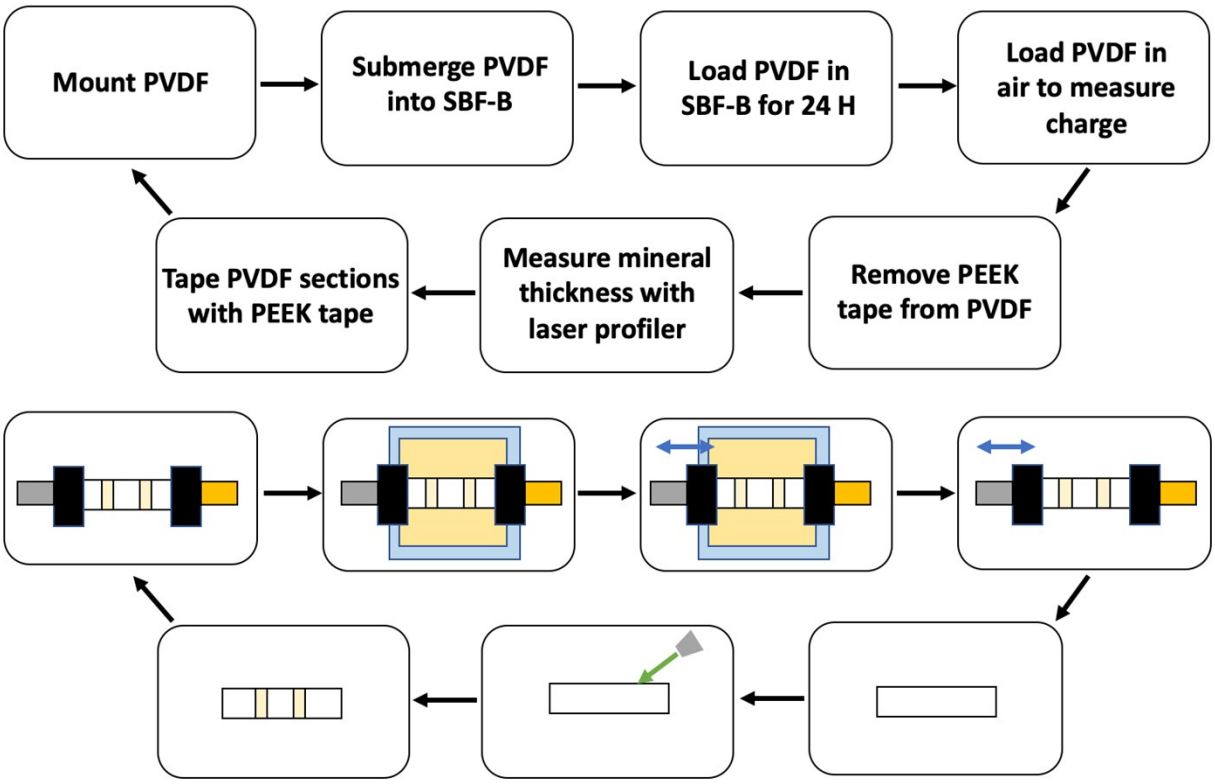

Fig. S4 Mineral growth and measurement procedure. The PVDF is mounted, submerged into SBF-B, and cyclically loaded to grow calcium-phosphate minerals. The PVDF is loaded in air to measure the charge, and the PEEK tape is removed to allow for laser profiling of the mineral thickness. The PVDF is then taped and the process is repeated multiple times until the maximum thickness is reached. The top row shows the description of the procedure and the bottom shows the schematic of the procedure.

Following the 24-hour growth period and measurements, the PVDF is mounted to the load cell and actuator before submerging the PVDF into a fresh solution of SBF-B. The growth process is repeated until the mineral thickness stops increasing.

III. Supplementary Note 3: Force Measurement Method

Force Measurement Method

The force on the cyclically loaded substrate was measured continuously during loading, both in the air to obtain charge measurements as well as in solution during mineralization. The force was measured using a force sensor (McMaster-Carr 3487N29) connected to a computer as in (Fig. S2). To obtain force values, the force was measured for 100 sec at a sampling rate of 1000 Hz by a load cell. Within each cycle, the maximum force was recorded, and the 200 maximum force values were combined to determine the average force at the given conditions with error bars representing the standard deviation of the measurements.

IV. Supplementary Note 4: Charge Measurement Method and Setup

Charge Distribution Data

The distribution of the generated piezoelectric charges across the surface of the PVDF was measured to determine an optimal location of the measurement charge probes. Under stressed conditions, the stress may not be equally distributed, and thus some locations may exhibit different local charges. To measure the charge distribution, the PVDF sample was divided into five zones with PEEK tape as shown in (Fig. S5). The charge probes were placed within one zone of the sample, and the sample was cyclically loaded in the air. The charge was measured 12 times within each zone, and the centermost region zone 3 produced statistically significantly larger charge magnitudes than the other zones probably due to minimum boundary effects.

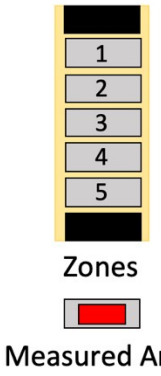

Zone	Charge (pC)
Zone 1	10.3 ± 0.1
Zone 2	12.1 ± 0.3
Zone 3	13.4 ± 0.4
Zone 4	11.1 ± 0.2
Zone 5	10.7 ± 0.3

Fig. S5 Charge distribution of a PVDF sample. The sample is divided into five zones and measured under identical cyclic loading conditions in air.

For the experimental measurements, the effective charges were measured within zone 3 as shown in (Fig. S6) in order to minimize variations due to non-uniform stress distribution.

Charge Measurement Method

The effective charge of the PVDF sample was measured before nucleation and again after every 24 hours of mineralization. To measure the effective charge, the sample was attached to the electrodynamic shaker, but the sample remained suspended in air as in (Fig. S3). The sample was then dried to prevent conduction between the charge probes. The PEEK tape attached to create unmineralized areas remained on the PVDF surface. Two probe electrodes were attached to the sample and connected to a charge amplifier (Measurement Specialties 1007214) that was connected to a data acquisition board (National Instruments BNC-2110). The charge probes were attached in the center region of the sample between the PEEK tape as shown in (Fig. S6a) to ensure consistent charge measurements as the charge had a measurable distribution that decreased from a peak in the center of the sample to minimums at the vertical and lateral edges. To secure the probes and ensure consistent contact pressure between the probes and sample as well as prevent lateral movement of the probes, a clip (MEETOOT B09L71CCD) was placed as shown in (Fig. S6b). The samples were then cyclically loaded under the same loading conditions as the mineral growth loading period to generate the same underlying piezoelectric charge. The outputs were read by an attached computer and a LabVIEW program was used to convert the outputs into charge measurements. For each sample and timepoint, the charge was measured twelve times in the same location. The measured charge magnitude is the effective charge magnitude that reaches through the mineral layer. To obtain the charge values, 12 charge measurements of 2 seconds each were sampled at a rate of 2000 Hz by a piezoelectric charge amplifier. Within each measurement, the maximum charge was recorded, and the 12 maximum charge values were combined to determine the average charge at the given conditions with error bars representing the standard deviation of the measurements.

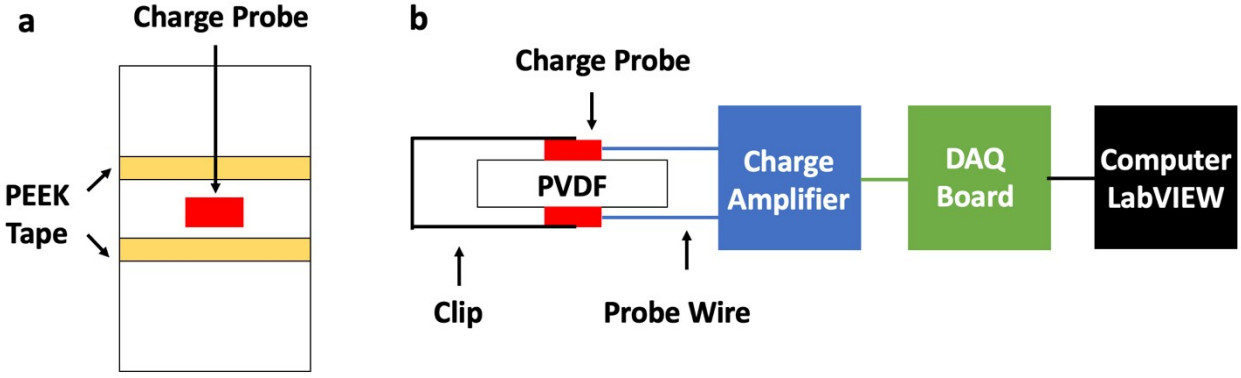

Fig. S6 Schematics of a charge measurement setup. (a) Top view of the charge measurement setup, with the charge probes placed in the center of the sample. (b) Side view of the charge measurement setup, the charge probes are secured with a clip and connected to a charge amplifier, data acquisition board, and computer.

Following charge measurements, the sample was removed from the electrodynamic shaker and prepared for thickness measurements by removing the PEEK tape.

V. Supplementary Note 5: Mineral Thickness Distribution and Measurement Method

Thickness Distribution

The distribution of the formed mineral thickness across the surface of the PVDF piezoelectric substrate was measured to determine an optimal and reliable method of obtaining accurate thickness values across multiple measurement time points. Cyclic loading may not distribute the stress equally across the surface of the PVDF, and the effective charge may vary across the surface of the PVDF. Due to this, there is a high likelihood that the mineral thickness, being closely related to the magnitude of the effective charges and stress, will vary across the surface of the PVDF.
To measure the thickness distribution, the PVDF sample was divided into five zones with PEEK tape as shown in (Fig. S7). The sample was seeded in SBF-A solution for 24-hour at 25 °C without any cyclic loading. The solution was then replaced with SBF-B, and the sample was loaded for 24-hour at 25 °C to induce mineral formation. The sample was then removed from the SBF-B solution and dried before removing the PEEK tape to expose the unmineralized areas for measurement. The sample was measured using a Keyence laser profilometer (Keyence VK-X100). The mineral thickness was measured in ten specific areas around each of the five zones as shown in Figure S7. Each of the fifty total areas was scanned and measured in five locations for a total of 250 measurements. The thickness was found to be at a maximum at the center of the sample, and decreased both laterally and vertically moving away from the center. There was also no statistically significant difference in thickness values within 3 mm laterally and 10 mm vertically from the center of the sample.

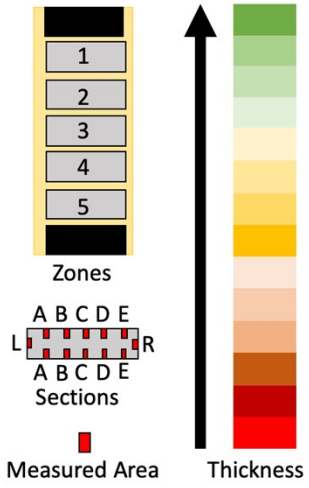

Average Mineral Thickness (µm)							
Zone	Left End	Section A	Section B	Section C	Section D	Section E	Right End
1	37.4 ± 2.7	46.9 ± 8.1	70.8 ± 12.3	79.1 ± 4.0	78.1 ± 4.2	57.7 ± 7.4	43.0 ± 2.1
		76.3 ± 9.6	76.7 ± 7.0	90.1 ± 3.3	82.2 ± 7.8	74.8 ± 6.3	
2	31.9 ± 1.8	67.7 ± 7.6	67.2 ± 8.7	94.0 ± 3.4	82.2 ± 3.1	75.5 ± 7.0	42.3 ± 2.9
		87.7 ± 8.2	90.1 ± 7.2	97.1 ± 6.1	85.2 ± 3.9	82.5 ± 7.9	
3	38.5 ± 1.5	67.8 ± 6.2	93.0 ± 9.5	99.1 ± 9.5	91.7 ± 8.6	81.5 ± 3.7	40.4 ± 3.6
		72.8 ± 2.9	89.8 ± 8.5	103.8 ± 8.2	91.0 ± 3.0	90.6 ± 4.2	
4	32.5 ± 2.1	66.2 ± 4.5	80.0 ± 5.1	94.1 ± 5.4	80.1 ± 5.6	77.2 ± 4.5	40.5 ± 3.9
		66.5 ± 4.3	84.5 ± 6.4	95.2 ± 6.2	85.3 ± 5.8	80.4 ± 8.3	
5	37.4 ± 1.9	68.8 ± 2.2	79.0 ± 3.7	85.4 ± 5.3	79.3 ± 6.6	75.7 ± 1.9	42.5 ± 4.7
		63.6 ± 6.3	84.5 ± 2.6	94.7 ± 7.1	77.6 ± 8.1	72.3 ± 8.7	

Fig. S7 Mineral thickness distribution of a PVDF substrate. The thickness of the minerals decreases with increasing distance from the center of the sample. The schematics show the location of the measured section and the zone of a sample.

For the experimental measurements, the mineral thickness was measured as shown in (Fig. S8) to minimize variations due to thickness distributions between measurements.

Thickness Measurements Method

The calcium-phosphate mineral thickness was measured after every 24-hour of mineralization. To measure the mineral thickness, the sample was removed from the electrodynamic shaker and the PEEK tape was removed to expose the unmineralized reference sections. Then, the sample was dried before measuring the mineral thickness using a Keyence laser profilometer (Keyence VK-X100). The mineral thickness was measured in four specific areas along the unmineralized regions as shown in (Fig. S8). These areas were defined to be within 3 mm in either direction of the center of the sample along the mineral boundaries. These areas were chosen due to no statistically significant difference in thickness measurements being found up to 10 mm vertically from the center of the sample and up to 5 mm laterally from the center of the sample. To sample the area, the four mineral edge regions were scanned in three zones each. Thickness values were obtained from the 12 locations on the film measured 5 times each with a laser profilometer.

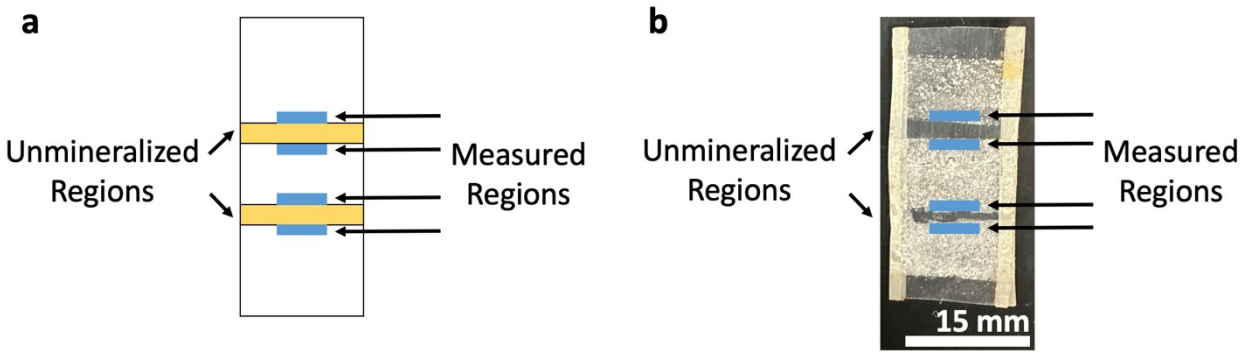

Fig. S8 Thickness measurement method. (a) Top view of the thickness measurement areas, with the thickness measured along the edges of the unmineralized regions. (b) Top view of a dried mineralized PVDF sample with the thickness laser profiled in the highlighted measured regions.

Within each measurement, the maximum mineral thickness was recorded, and the 60 maximum thickness values were combined to determine the average thickness at the given condition with error bars representing the standard deviation of the measurements.

VI. Supplementary Note 6: Images of Minerals During Growth Process

Microscopic Images of Minerals During Growth

Microscopic images were taken during thickness measurements using a Keyence laser profilometer (Keyence VK-X100). Five zones were imaged corresponding with the five zones as shown in Figure S7. Images of the formed minerals at 24 hours of mineral growth and after reaching steady state mineral thickness are shown in Figure S9. Visual inspection indicates full coverage of the sample surface after 24 hours of mineral growth, with no striking differences in morphology as a function of loading force.

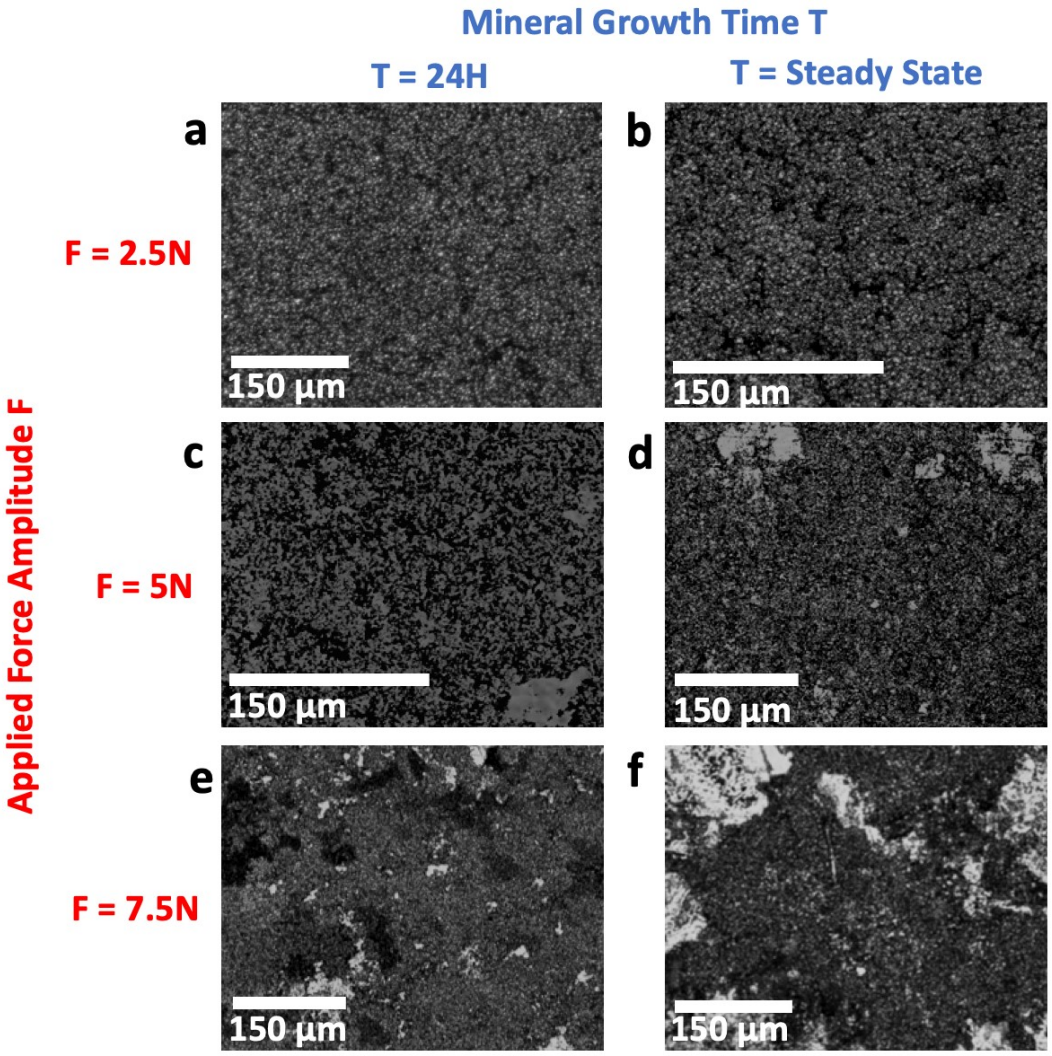

Fig. S9 Optical microscope images of minerals formed after 24 hours and steady state thickness. (a) Minerals formed under 2.5 N loading amplitude cyclic stress after 24 hours of nucleation and 24 hours of mineral growth. (b) Minerals formed under 2.5 N loading amplitude cyclic stress after 24 hours of nucleation and 48 hours of mineral growth (after reaching steady state mineral thickness). (c) Minerals formed under 5 N loading amplitude cyclic stress after 24 hours of nucleation and 24 hours of mineral growth. (d) Minerals formed under 5 N loading amplitude cyclic stress after 24 hours of nucleation and 48 hours of mineral growth (after reaching steady state mineral thickness.) (e) Minerals formed under 7.5 N loading amplitude cyclic stress after 24 hours of nucleation and 24 hours of mineral growth. (f) Minerals formed under 7.5 N loading amplitude cyclic stress after 24 hours of nucleation and 48 hours of mineral growth (after reaching steady state mineral thickness). Due to removing and drying the samples for charge and thickness measurements, partial delamination of samples occurs during repeated cycles for longer duration experiments as visible in (e) and (f).

VII. Supplementary Note 7: Mineral Thickness at Different Growth Temperatures

Ultimate Mineral Thickness at Different Growth Temperatures

The temperature dependence of the self-limiting growth mechanism was studied by mineralizing unloaded samples until steady state mineral thickness was reached at a temperature range of 25–50°C. In this case, the driving force for mineralization was due to the inherent charges present on the piezoelectric substrates. In these experiments, there was no statistically significant difference in the ultimate film thickness as a function of temperature, nor was there a statistically significant difference in the mineral thickness between samples mineralized at the same temperature. The measurement results are summarized in Table S2 and shown in Figure S10. This indicates that the ultimate mineral thickness is dependent on and controllable by force, and further validates our model indicating that the charge magnitude is the primary driving force and is reduced predominantly by distance from the charge source. In addition, previous studies indicated that the initial film growth rate was strongly correlated with temperature over the initial 24 hours of film growth. This could indicate that the speed of the film growth can be accelerated with increasing temperature, but the mineral thickness will eventually converge to the same ultimate thickness.

Table S2: Ultimate mineral thickness in unloaded samples grown at different temperatures.

Temperature (°C)	Mineral Thickness (μm)	T-Test Pairs	P Value
25	58.92 ± 12.90	25°C / 37.5°C	0.64
37.5	57.55 ± 9.88	37.5°C / 50°C	0.83
50	58.11 ± 9.35	25°C / 50°C	0.81

Each sample was nucleated for 24 hours with SBF-A, and then grown in SBF-B at the listed temperature. The samples remained unloaded during nucleation and growth, and the solution was refreshed every 24 hours. Two samples were grown at each temperature conditions, and the mineral thickness for each sample was measured 15 times.

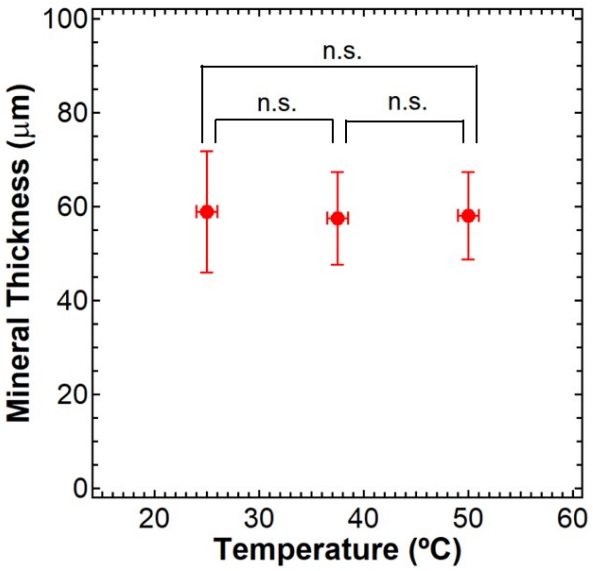

Fig. S10 Ultimate mineral thickness in unloaded samples as a function of growth temperature. Measured thickness values after reaching steady state growth indicate no statistically significant differences between samples grown at different temperatures at least within the measurement range. Previous studies indicate that the initial growth rate is dependent on temperature, but at steady state the mineral thickness converges to the same value.

VIII. Supplementary Note 8: Compatibility of Ionic Compounds

Compounds feasible to form with seawater, blood plasma, SBF, and additional fluid compositions

The ionic composition of seawater, blood plasma, and simulated body fluid utilized in the study are listed in Table S3. The feasible compounds to form utilizing these fluids are shown in Table S4. Additional ionic compounds that could be formed with the addition of further ionic species as well as the needed ions are available in Table S5.

Table S3: Ionic composition of seawater, blood plasma, and SBF[1–3,5].

Fluid	**Concentration (mM)**									
Species	Na^+	K^+	Ca^{2+}	Mg^{2+}	HCO_3^-	Cl^-	SO_4^-	Sr^{2+}	Li^+	PO_4
Seawater	479	10.4	10.5	54.3	2.0	558	28.9	0.09	0.026	<0.003
Blood Plasma	142	5.0	2.5	1.5	27.0	103	-	-	-	1.0
10x SBF-A	1430	-	25	15.0	42	1470	-	-	-	10
10x SBF-B	1408	-	25	3.0	21	1436	-	-	-	10

The ionic components present in seawater, blood plasma, 10x SBF-A (nucleation solution), and 10x SBF-B (growth solution) as well as the corresponding concentrations of each species present in the fluids is listed.

Table S4: Examples of ionic compounds able to be formed from seawater, blood plasma, and SBF[5].

Group	Compound Name	Chemical Formula	Possible Fluid
Carbonates	Calcite	$CaCO_3$	Seawater, blood, SBF
	Aragonite	$CaCO_3$	Seawater, blood, SBF
	Mg-calcite	$(Mg_xCa_{1-x})CO_3$	Seawater, blood, SBF
	Vaterite	$CaCO_3$	Seawater, blood, SBF
	Monohydrocalcite	$CaCO_3•H_2O$	Seawater, blood, SBF
	Protodolomite	$CaMg(CO_3)_2$	Seawater, blood, SBF
	Amorphous calcium carbonate	$CaCO_3$	Seawater, blood, SBF
Phosphates	Octacalcium phosphate	$Ca_8H_2(PO_4)_6$	Blood, SBF
	Hydroxyapatite	$Ca_{10}(PO_4)_6(OH)_2$	Blood, SBF
	Apatite	$Ca_5(PO_4)$	Blood, SBF
	Brushite	$CaHPO_4•2H_2O$	Blood, SBF
	Dahllite	$Ca_5(PO_4,CO_3)_3(OH)$	Blood, SBF
	Amorphous calcium phosphate	$CaxH_y(PO_4)_z•nH_2O$	Blood, SBF
	Amorphous calcium pyrophosphate	$Ca_2P_2O_7•2H_2O$	Blood, SBF
Sulfates	Gypsum	$CaSO_4•2H_2O$	Seawater
	Celestite	$SrSO_4$	Seawater
Organic crystals	Calcium tartrate	$C_4H_4CaO_6$	Seawater, blood, SBF
	Calcium malate	$C_4H_4CaO_5$	Seawater, blood, SBF
	Earlandite	$Ca_3(C_6H_5O_2)_2•4H_2O$	Seawater, blood, SBF
	Whewellite	$CaC_2O_4•H_2O$	Seawater, blood, SBF
	Weddelite	$CaC_2O_4•(2+X)H_2O$ $(X<0.5)$	Seawater, blood, SBF
	Glushinskite	$MgC_2O_4•4H_2O$	Seawater, blood, SBF

Ionic compounds and their chemical formulas that could be formed from seawater, blood plasma, and SBF are listed. For each compound, the chemical formula and feasible existing fluid to synthesize the compound is listed.

Table S5: Examples of ionic compounds potentially possible to form from additional ionic solution compositions[5].

Group	Compound Name	Chemical Formula	Additional Components
Carbonates	Hydrocerussite	$Pb_3(CO_3)_2(OH)_2$	Pb
Phosphates	Francolite	$Ca_{10}(PO_4)_6F_2$	F
Sulfates	Barite	$BaSO_4$	Ba
Sulfides	Pyrite	FeS_2	Fe
	Hydrotroilite	$FeS•nH_2O$	Fe
	Sphalerite	ZnS	Zn
	Wurtzite	ZnS	Zn
	Galena	PbS	Pb
	Greigite	Fe_3S_4	Fe
	Mackinawite	$(Fe,Ni)_9S_8$	Fe, Ni
	Amorphous pyrrhotite	$Fe_{1-x}S$ (x = 0-0.17)	Fe
	Acanthite	Ag_2S	Ag
Arsenates	Orpiment	As_2S_3	As
Hydrated silica	Amorphous silica	$SiO_2•nH_2O$	Si
Chlorides	Atacamite	$Cu_2Cl(OH)_3$	Cu
Fluorides	Fluorite	CaF_2	F
	Hieratite	K_2SiF_6	Si, F
Perovskites	Barium titanate	$BaTiO_3$	Ba, Ti
	Cesium lead iodide	$CsPbI_3$	Cs, Pb, I
Oxides	Magnetite	Fe_3O_4	Fe
	Amorphous ilmenite	$Fe^{+2}TiO_3$	Fe, Ti
	Amorphous iron oxide	Fe_2O_3	Fe
	Amorphous manganese oxide	Mn_3O_4	Mn
Organic crystals	Uric acid	$C_5H_4N_4O_3$	N
	Manganese oxalate	$Mn_2C_2O_4•4H_2O$	Mn
	Sodium urate	$C_5H_3N_4NaO_3$	N
	Guanine	$C_5H_3(NH_2)N_4O$	N
Hydroxides	Goethite	α-FeOOH	Fe
	Lepidocrocite	γ-FeOOH	Fe

Ionic compounds and their chemical formulas that could be formed through new formulations of surrounding ionic solutions via the addition of specific ions. For each compound, the additional needed ions not typically found in either seawater, blood plasma, or SBF is listed.

IX. Supplementary References

1 P. Habibovic, F. Barrère, C. A. Van Blitterswijk, K. De Groot, and P. Layrolle, *J. Am. Ceram. Soc.* 2002, **85**, 517-522.

2 A. C. Tas and S. B. Bhaduri, *J. Mater. Res.* 2004, **19**, 2742-2749.

3 K. Hata, T. Kokubo, T. Nakamura, and T. Yamamuro, *J. Am. Ceram. Soc.* 1995, **78**, 1049-1053.

4 S. Orrego, Z. Chen, U. Krekora, D. Hou, S. Y. Jeon, M. Pittman, C. Montoya, Y. Chen, and S. H. Kang, *Adv. Mater.,* 2020, **32**(1906970), 1-6.

5 Weiner, S. and Dove, P. M., *Rev. Mineral. Geochem.* 2003, **54**(1), 1-29.